MOLECULAR BIOLOGY

The inositol pyrophosphate 5-InsP₇ drives sodium-potassium pump degradation by relieving an autoinhibitory domain of PI3K p85α

Alfred C. Chin[1]*[†], Zhe Gao[2,3†], Andrew M. Riley[4], David Furkert[5], Christopher Wittwer[6], Amit Dutta[6], Tomas Rojas[1], Evan R. Semenza[1], Robin A. Felder[7], Jennifer L. Pluznick[8], Henning J. Jessen[6], Dorothea Fiedler[5], Barry V. L. Potter[4], Solomon H. Snyder[1,9,10‡], Chenglai Fu[2,3‡]

Sodium/potassium-transporting adenosine triphosphatase (Na⁺/K⁺-ATPase) is one of the most abundant cell membrane proteins and is essential for eukaryotes. Endogenous negative regulators have long been postulated to play an important role in regulating the activity and stability of Na⁺/K⁺-ATPase, but characterization of these regulators has been elusive. Mechanisms of regulating Na⁺/K⁺-ATPase homeostatic turnover are unknown. Here, we report that 5-diphosphoinositol 1,2,3,4,6-pentakisphosphate (5-InsP₇), generated by inositol hexakisphosphate kinase 1 (IP6K1), promotes physiological endocytosis and downstream degradation of Na⁺/K⁺-ATPase-α1. Deletion of IP6K1 elicits a twofold enrichment of Na⁺/K⁺-ATPase-α1 in plasma membranes of multiple tissues and cell types. Using a suite of synthetic chemical biology tools, we found that 5-InsP₇ binds the RhoGAP domain of phosphatidyl-inositol 3-kinase (PI3K) p85α to disinhibit its interaction with Na⁺/K⁺-ATPase-α1. This recruits adaptor protein 2 (AP2) and triggers the clathrin-mediated endocytosis of Na⁺/K⁺-ATPase-α1. Our study identifies 5-InsP₇ as an endogenous negative regulator of Na⁺/K⁺-ATPase-α1.

INTRODUCTION

Inositol phosphates are indispensable signaling molecules in animal and plant cells. D-*myo*-inositol 1,4,5-trisphosphate, the most studied inositol phosphate, releases calcium from intracellular stores (*1*). Higher inositol phosphates with energetic pyrophosphate bonds participate in essential cell signaling pathways by binding or pyrophosphorylating target proteins (*2*). 5-Diphosphoinositol 1,2,3,4,6-pentakisphosphate (5-InsP₇), which is generated by a family of three inositol hexakisphosphate kinases (IP6Ks), is the most abundant inositol pyrophosphate in mammalian cells (*3*). 5-InsP₇ regulates disparate cell biology processes, including nuclear dynamics, vacuole biogenesis, vesicular trafficking, cellular morphology, cell death, and growth factor and cytokine signaling (*4*, *5*). Deleting different IP6K isoforms elicits distinct phenotypes. *IP6K1* knockout (KO) mice are lean and resistant to high-fat–induced obesity, *IP6K2* KO mice are more susceptible to carcinogen-induced aerodigestive tract carcinoma, and *IP6K3* KO mice display impaired motor learning and coordination (*5*, *6*). Moreover, IP6Ks exhibit an isoform-specific cellular localization: IP6K1/K3 localizes to the cytoplasm and plasma membrane, whereas IP6K2 localizes to the nucleus (*7*, *8*). Both the distinct phenotypic regulation and the differential localization suggest a model whereby individual IP6Ks generate pools of 5-InsP₇ that function in discrete, localized areas where the kinase is enriched (*5*, *9*). To further understand the physiological function of IP6K1, we performed a gel-based proteomic screen of membrane proteins and found that deletion of IP6K1 elicits a twofold enrichment of Na⁺/K⁺-ATPase-α1 in the plasma membrane.

Na⁺/K⁺-transporting adenosine triphosphatase (Na⁺/K⁺-ATPase) is universally expressed in the plasma membrane of animal cells, constituting a substantial proportion of total membrane proteins and consuming a large percentage of cytoplasmic ATP (*10*). It generates electrochemical gradients across the cell membrane that are crucial for cell volume maintenance, signal transduction, and secondary transport of various nutrients (*11*). Steady-state turnover of Na⁺/K⁺-ATPase requires coordinated endocytosis from, and insertion into, the plasma membrane (*12*). Endocytosis of Na⁺/K⁺-ATPase under pathological conditions involves phosphorylation of the α subunit (*13*) and interaction with phosphatidylinositol 3-kinase (PI3K) p85α (*14*). Subsequently, adaptor protein 2 (AP2) is recruited to drive clathrin-mediated endocytosis (*15*) and downstream proteasomal and lysosomal degradation of Na⁺/K⁺-ATPase (*12*, *16*). However, the regulatory mechanisms controlling Na⁺/K⁺-ATPase homeostatic turnover are unclear. Furthermore, evidence for the existence of endogenous negative regulators of Na⁺/K⁺-ATPase, such as endogenous digitalis-like factors, has existed for decades (*17*), but the identification of such molecules has been elusive.

We now report that 5-InsP₇, generated by IP6K1, is an endogenous negative regulator of Na⁺/K⁺-ATPase-α1. 5-InsP₇ drives physiological endocytosis of Na⁺/K⁺-ATPase-α1 by binding with PI3K p85α to disinhibit the interaction of PI3K p85α with Na⁺/K⁺-ATPase-α1. This recruits AP2, leading to clathrin-mediated endocytosis and downstream degradation of Na⁺/K⁺-ATPase-α1.

[1]The Solomon H. Snyder Department of Neuroscience, Johns Hopkins University School of Medicine, Baltimore, MD, USA. [2]Tianjin Key Laboratory of Metabolic Diseases, Department of Physiology and Pathophysiology, Tianjin Medical University, Tianjin, China. [3]Key Laboratory of Immune Microenvironment and Disease (Ministry of Education), Tianjin Medical University, Tianjin, China. [4]Medicinal Chemistry and Drug Discovery, Department of Pharmacology, University of Oxford, Oxford, UK. [5]Leibniz-Forschungsinstitut für Molekulare Pharmakologie, Berlin, Germany. [6]Institute of Organic Chemistry and CIBSS—Centre for Integrative Biological Signalling Studies, University of Freiburg, D-79104 Freiburg, Germany. [7]Department of Pathology, University of Virginia, Charlottesville, VA, USA. [8]Department of Physiology, Johns Hopkins University School of Medicine, Baltimore, MD, USA. [9]Department of Pharmacology and Molecular Sciences, Johns Hopkins University School of Medicine, Baltimore, MD, USA. [10]Department of Psychiatry and Behavioral Sciences, Johns Hopkins University School of Medicine, Baltimore, MD, USA.
*Present address: Weill Cornell/Rockefeller/Sloan Kettering Tri-Institutional MD-PhD Program, New York, NY, USA.
†These authors contributed equally to this work.
‡Corresponding author. Email: ssnyder@jhmi.edu (S.H.S.); chenglaifu@tmu.edu.cn (C.F.)

RESULTS

Deletion of IP6K1 elicits a twofold increase in Na⁺/K⁺-ATPase-α1

We previously found that IP6K1 is enriched in the plasma membrane (8) and wondered whether its deletion alters protein expression in the cell membrane. We isolated cell membrane fractions of wild-type (WT) and *IP6K1* KO mouse embryonic fibroblast (MEF) cells and compared protein levels by gel electrophoresis and silver staining (Fig. 1A). One protein band at molecular weight ~100 kDa was notably darker in *IP6K1* KO preparation, suggesting an increased expression (Fig. 1A). Mass spectrometry identified the protein as Na⁺/K⁺-ATPase-α1. The increase of Na⁺/K⁺-ATPase-α1 in *IP6K1* KO MEFs was confirmed by Western blot, confirming that IP6K1 negatively regulates Na⁺/K⁺-ATPase-α1 protein level (Fig. 1, B and C). Knocking down IP6K1 by short hairpin RNA (shRNA) in human renal proximal tubule cells (hRPTCs) elicited a substantial increase of Na⁺/K⁺-ATPase-α1 in the plasma membrane, as shown by confocal microscopy (fig. S1A). The Na⁺/K⁺-ATPase is principally composed of α and β subunits. The α subunit is catalytic, and the β subunit is regulatory and acts as a chaperone to facilitate trafficking of α subunits to the plasma membrane. The α1/β1 complex is the principal Na⁺/K⁺-ATPase expressed in virtually every tissue (18). We examined Na⁺/K⁺-ATPase-α1 and Na⁺/K⁺-ATPase-β1 protein levels in WT and *IP6K1* KO animals. Consistently, deletion of IP6K1 markedly increased Na⁺/K⁺-ATPase-α1 in the kidneys (fig. S1B), brains (fig. S1C), and hearts (fig. S1D). Together with Na⁺/K⁺-ATPase-α1, the Na⁺/K⁺-ATPase-β1 subunit was also increased in the *IP6K1* KO tissues (fig. S1, B to D). We isolated the cell membrane fractions of WT and *IP6K1* KO kidneys. Increased expression of Na⁺/K⁺-ATPase-α1 in the cell membrane of *IP6K1* KO kidneys was confirmed by Western blot (Fig. 1D). Conversely, overexpressing IP6K1 drastically decreased Na⁺/K⁺-ATPase-α1 protein levels in hRPTCs (Fig. 1E). The β1 subunit was also increased in the *IP6K1* KO cell membrane (Fig. 1D) and decreased in the IP6K1-overexpressing hRPTCs (Fig. 1E). Thus, IP6K1 negatively regulates Na⁺/K⁺-ATPase-α1 protein level.

We wondered whether the protein level of Na⁺/K⁺-ATPase-α1 is also regulated by other isoforms of IP6K. We performed reverse transcription polymerase chain reaction (RT-PCR) to confirm the expressions of IP6K1, IP6K2, and IP6K3 in hRPTCs (fig. S2A) and mouse kidneys (fig. S2B). We compared the protein levels of Na⁺/K⁺-ATPase-α1 and Na⁺/K⁺-ATPase-β1 in WT and *IP6K2* KO kidneys. Deletion of IP6K2 did not alter Na⁺/K⁺-ATPase-α1 and Na⁺/K⁺-ATPase-β1 protein levels (fig. S2, C and D). The expression levels of IP6K3 in hRPTCs and mouse kidneys were negligible compared to those of IP6K1 and IP6K2, suggesting that IP6K3 does not play a major role (fig. S2, A and B). Thus, Na⁺/K⁺-ATPase-α1 is specifically regulated by IP6K1.

Increased Na⁺/K⁺-ATPase-α1 drives fluid retention in *IP6K1* KO animals

IP6K1 is highly expressed in the basolateral side of renal tubule cells (fig. S3A), where Na⁺/K⁺-ATPase-α1 is localized (Fig. 1F). Knocking out IP6K1 depleted its expression in kidneys (fig. S3B) and sharply increased Na⁺/K⁺-ATPase-α1 protein level in the basolateral membrane of the renal tubule cells (Fig. 1F). Correspondingly, the Na⁺/K⁺-ATPase pump activity was elevated in *IP6K1* KO kidneys, albeit proportionally less than that of protein level elevation (Fig. 1G). This may be attributed to a nonpumping pool of Na⁺/K⁺-ATPase-α1 (19) or an unknown compensatory mechanism. Because IP6K1 ex-pression in the glomerulus is negligible (fig. S3A), deletion of IP6K1 did not increase the staining of Na⁺/K⁺-ATPase-α1 in glomerulus (Fig. 1F).

We explored the physiological relevance of the increased Na⁺/K⁺-ATPase-α1 in *IP6K1* KO kidneys by assessing Na⁺ reabsorption, which can be reflected by renal Na⁺ excretion (Fig. 1, H and I). Daily salt and water consumptions were similar between WT and *IP6K1* KO mice (fig. S4, A to D). However, daily urinary Na⁺ excretion in *IP6K1* KO mice was substantially less than that of WT mice when the animals were fed a high-salt (HS) diet (4% NaCl) (Fig. 1H), but it was similar between WT and *IP6K1* KO mice on normal-salt (NS) diet (0.2% NaCl) (Fig. 1I). This result indicates fluid retention in the HS diet–fed *IP6K1* KO mice. After a 9-week HS diet, the *IP6K1* KO mice gained a significant amount of weight compared with a separate cohort of age-matched NS diet–fed *IP6K1* KOs (Fig. 1J). In contrast, the HS diet–fed WT mice did not gain weight (Fig. 1K). The increased Na⁺ reabsorption and fluid retention in *IP6K1* KO mice establishes a functional role of IP6K1-regulated Na⁺/K⁺-ATPase-α1 stability. Notably, *IP6K1* KO mice have lower body weights than WT littermates, which has been proposed to result from higher energy expenditure of *IP6K1* KOs (20). Because Na⁺/K⁺-ATPase consumes more than 25% of cellular ATP, the increased Na⁺/K⁺-ATPase-α1 may partially contribute to the higher energy expenditure observed in the *IP6K1* KO animals.

Blood urea nitrogen levels were similar between WT and *IP6K1* KO mice (fig. S4E), and the blood creatinine level was higher in *IP6K1* KO mice (fig. S4F), which may be attributable to higher muscle mass in *IP6K1* KO mice (20). Time-inulin concentration curves were similar between WT and *IP6K1* KO mice, suggesting similar glomerular filtration rates (fig. S4G). No obvious renal pathology was observed in the *IP6K1* KO mice by hematoxylin and eosin (H&E) (fig. S5A), periodic acid–Schiff (PAS) (fig. S5B), and Masson (fig. S5C) staining.
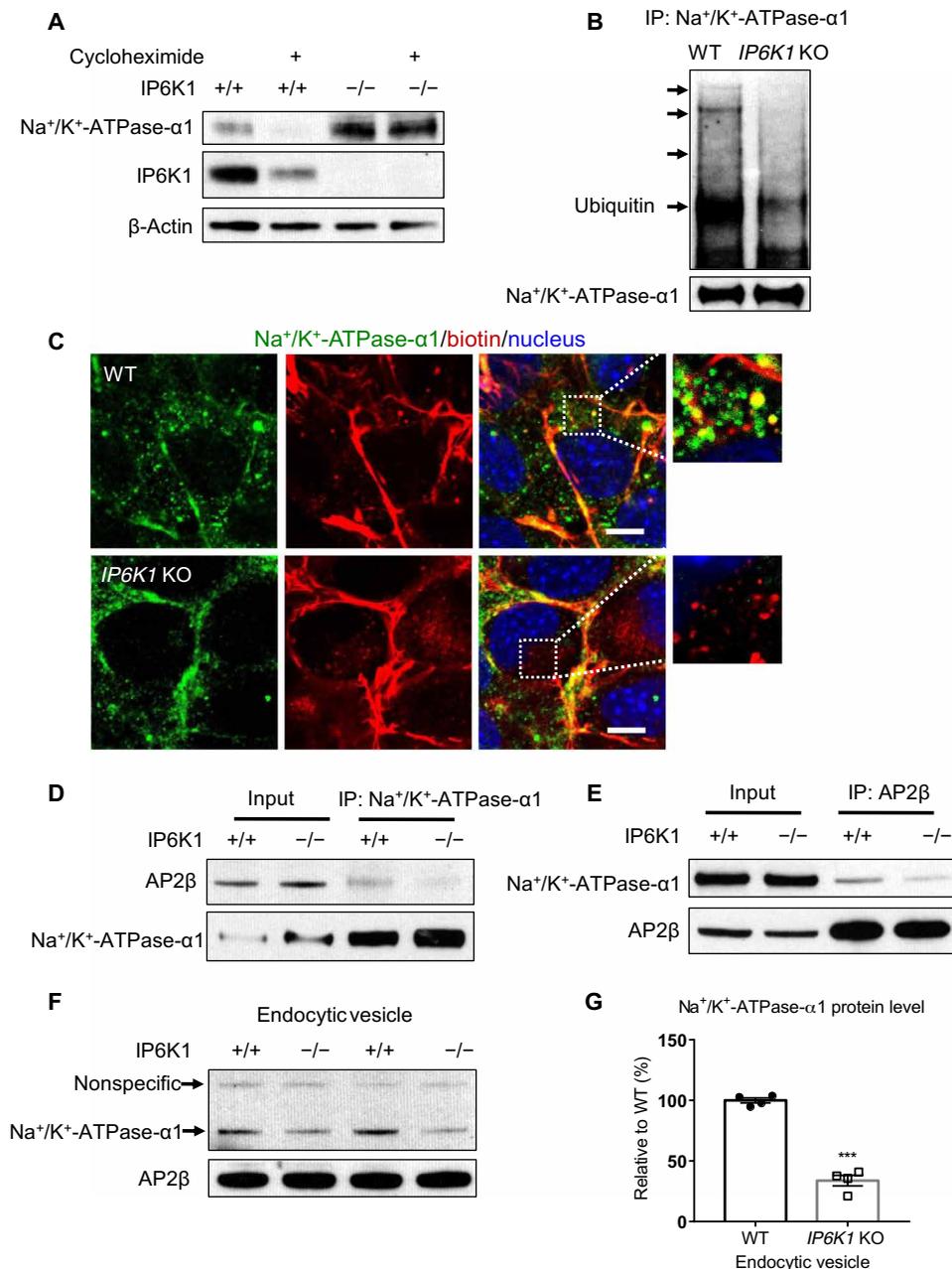
Deletion of IP6K1 impairs endocytosis and degradation of Na⁺/K⁺-ATPase-α1

To dissect the mechanism by which IP6K1 regulates Na⁺/K⁺-ATPase-α1, we tested the transcription levels of Na⁺/K⁺-ATPase-α1 in WT and *IP6K1* KO kidneys and MEF cells (fig. S6, A and B). The mRNA level of Na⁺/K⁺-ATPase-α1 was reduced in *IP6K1* KO kidneys (fig. S6A), and the mRNA levels of Na⁺/K⁺-ATPase-α1 were similar in WT and *IP6K1* KO MEF cells (fig. S6B).

To determine how IP6K1 regulates Na⁺/K⁺-ATPase-α1 protein levels, we first tested the protein stability of Na⁺/K⁺-ATPase-α1 in WT and *IP6K1* KO cells. Using cycloheximide to stop protein synthesis, we found that Na⁺/K⁺-ATPase-α1 protein degradation was much slower in *IP6K1* KO cells than in WTs (Fig. 2A). Because internalized Na⁺/K⁺-ATPase-α1 is ubiquitinated before degradation (12, 16), we immunoprecipitated Na⁺/K⁺-ATPase-α1 from WT and *IP6K1* KO tissues to determine its ubiquitination status. Deletion of IP6K1 disrupted Na⁺/K⁺-ATPase-α1 ubiquitination (Fig. 2B), confirming that IP6K1 is required for Na⁺/K⁺-ATPase-α1 degradation. Na⁺/K⁺-ATPase is physiologically endocytosed and subsequently degraded under steady-state conditions (12). We then asked whether IP6K1 decreases the level of Na⁺/K⁺-ATPase-α1 protein by mediating its endocytosis. We labeled cell membrane proteins with biotin and incubated the cells at 37°C for 4 hours before staining Na⁺/K⁺-ATPase-α1. In WT preparations, colocalization of Na⁺/K⁺-ATPase-α1 with biotin was observed in the cytosol, indicative of normal
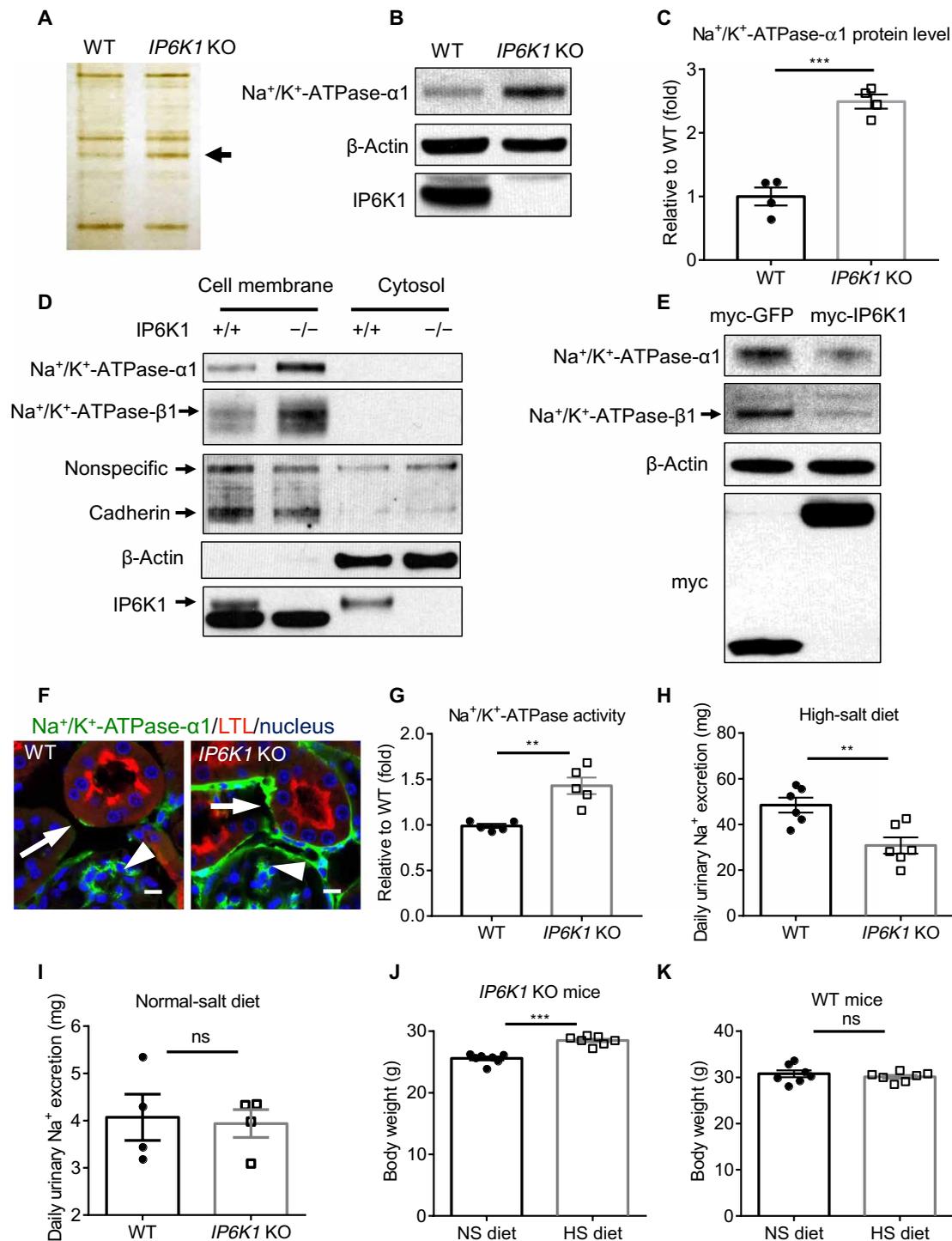
Fig. 1. Deletion of IP6K1 elicits a twofold increase in Na$^+$/K$^+$-ATPase-α1. (**A**) Plasma membrane fractions were isolated from WT and *IP6K1* KO MEFs. Silver stain revealed an enriched protein, Na$^+$/K$^+$-ATPase-α1, at ~100 kDa in *IP6K1* KO preparations (arrow). (**B** and **C**) Na$^+$/K$^+$-ATPase-α1 protein level was increased in whole-cell lysates of *IP6K1* KO MEFs ($n = 4$; normalized to β-actin). (**D**) Na$^+$/K$^+$-ATPase-α1 and Na$^+$/K$^+$-ATPase-β1 protein levels in plasma membrane fractions of kidneys were increased in *IP6K1* KOs. (**E**) Overexpression of myc-tagged IP6K1 decreased Na$^+$/K$^+$-ATPase-α1 and Na$^+$/K$^+$-ATPase-β1 protein levels in hRPTCs. (**F**) Immunostaining of Na$^+$/K$^+$-ATPase-α1 in WT and *IP6K1* KO kidneys. Fluorescein-labeled *Lotus tetragonolobus* Lectin (LTL) stained brush border of proximal tubule cells, and Hoechst 33342 labeled nucleus. Na$^+$/K$^+$-ATPase-α1 is selectively increased in the renal tubule cells (arrows) but not in the glomerulus (arrowheads) of *IP6K1* KOs. (**G**) Deletion of IP6K1 increased Na$^+$/K$^+$-ATPase activity ($n = 5$; normalized to WT mean). (**H** and **I**) WT and *IP6K1* KO mice were fed with high-salt (HS) diet (H) or normal-salt (NS) diet (I) for 9 weeks. (H) Daily urinary Na$^+$ excretion of HS diet–fed *IP6K1* KO mice was less than that of HS diet–fed WT ($n = 6$). (I) Daily urinary Na$^+$ excretions in NS diet–fed mice were similar ($n = 4$). (**J** and **K**) Age-matched *IP6K1* KO (J) and WT (K) mice were fed with HS or NS diet for 9 weeks. (J) HS diet–fed *IP6K1* KO mice gained weight ($n = 7$). (K) HS diet–fed WT mice did not gain weight ($n = 7$).

Fig. 2. Deletion of IP6K1 disrupts physiological endocytosis and degradation of Na$^+$/K$^+$-ATPase-α1. (**A**) WT and *IP6K1* KO MEF cells were treated with cycloheximide (100 μM) for 16 hours to stop protein synthesis. Dimethyl sulfoxide (DMSO) was used as a solvent control. Deletion of IP6K1 slowed down Na$^+$/K$^+$-ATPase-α1 degradation. (**B**) Na$^+$/K$^+$-ATPase-α1 in WT and *IP6K1* KO mice kidneys was immunoprecipitated (IP) and blotted for ubiquitin. Deletion of IP6K1 reduced Na$^+$/K$^+$-ATPase-α1 ubiquitination. (**C**) Cell membrane proteins of WT and *IP6K1* KO MEF cells were labeled with biotin. The cells were incubated at 37°C for 4 hours then fixed with 4% paraformaldehyde. Na$^+$/K$^+$-ATPase-α1 was immunostained, and biotin was labeled with fluorescent streptavidin. In WT cells, colocalization of Na$^+$/K$^+$-ATPase-α1 with biotin was observed in the cytoplasm (inset), indicating normal endocytosis. In *IP6K1* KO cells, biotin was observed in the cytoplasm (inset), but Na$^+$/K$^+$-ATPase-α1 remained in the cell membrane, suggesting that endocytosis of Na$^+$/K$^+$-ATPase-α1 was disrupted. Scale bars, 10 μm. (**D** and **E**) Coimmunoprecipitation of Na$^+$/K$^+$-ATPase-α1 and AP2β from WT and *IP6K1* KO kidneys. (D) Less AP2β was co–pulled down by Na$^+$/K$^+$-ATPase-α1 in *IP6K1* KOs. (E) Less Na$^+$/K$^+$-ATPase-α1 was coprecipitated by AP2β in *IP6K1* KOs. (**F**) Endocytic vesicles of WT and *IP6K1* KO kidneys were isolated and blotted for Na$^+$/K$^+$-ATPase-α1. The *IP6K1* KO endocytic vesicles contained less amount of Na$^+$/K$^+$-ATPase-α1, suggesting that endocytosis of Na$^+$/K$^+$-ATPase-α1 was disrupted. (**G**) Quantification of Na$^+$/K$^+$-ATPase-α1 protein levels in endocytic vesicles of WT and *IP6K1* KO kidneys ($n = 4$; normalized to AP2β).

endocytosis of Na$^+$/K$^+$-ATPase-α1. In contrast, in *IP6K1* KO cells, biotin was evident in the cytosol, but Na$^+$/K$^+$-ATPase-α1 remained enriched in the cell membrane, suggesting that endocytosis of Na$^+$/K$^+$-ATPase-α1 was disrupted (Fig. 2C).

Internalization of Na$^+$/K$^+$-ATPase-α1 requires its binding with AP2 (*15*). We performed coimmunoprecipitation to confirm that Na$^+$/K$^+$-ATPase-α1 and AP2 bind in WT tissues. In *IP6K1* KO tissues, binding between Na$^+$/K$^+$-ATPase-α1 and AP2 was markedly

diminished (Fig. 2, D and E), suggesting that deletion of IP6K1 impairs physiological endocytosis of Na$^+$/K$^+$-ATPase-α1. This was further confirmed by the fact that the endocytic vesicles isolated from *IP6K1* KO tissues contained substantially less amount of Na$^+$/K$^+$-ATPase-α1 than those from WTs (Fig. 2, F and G).

5-InsP$_7$ promotes Na$^+$/K$^+$-ATPase-α1 endocytosis
We wondered whether degradation of Na$^+$/K$^+$-ATPase-α1 promoted by IP6K1 relies on its enzymatic synthesis of 5-InsP$_7$. We rescued

IP6K1 KO MEF cells with lentiviral transduction of WT IP6K1 or kinase-deficient mutant (mut) IP6K1. The level of Na$^+$/K$^+$-ATPase-α1 protein was reduced by WT but not by mut IP6K1 (Fig. 3, A and B), suggesting that regulation of Na$^+$/K$^+$-ATPase-α1 by IP6K1 requires its enzymatic activity. We further confirmed this result by showing that pharmacological inhibition of 5-InsP$_7$ synthesis by N^2-(m-(trifluoromethyl)benzyl)N^6-(p-nitrobenzyl)purine (TNP) (21) increased Na$^+$/K$^+$-ATPase-α1 protein levels (Fig. 3C). TNP also dose-dependently diminished Na$^+$/K$^+$-ATPase-α1 ubiquitination
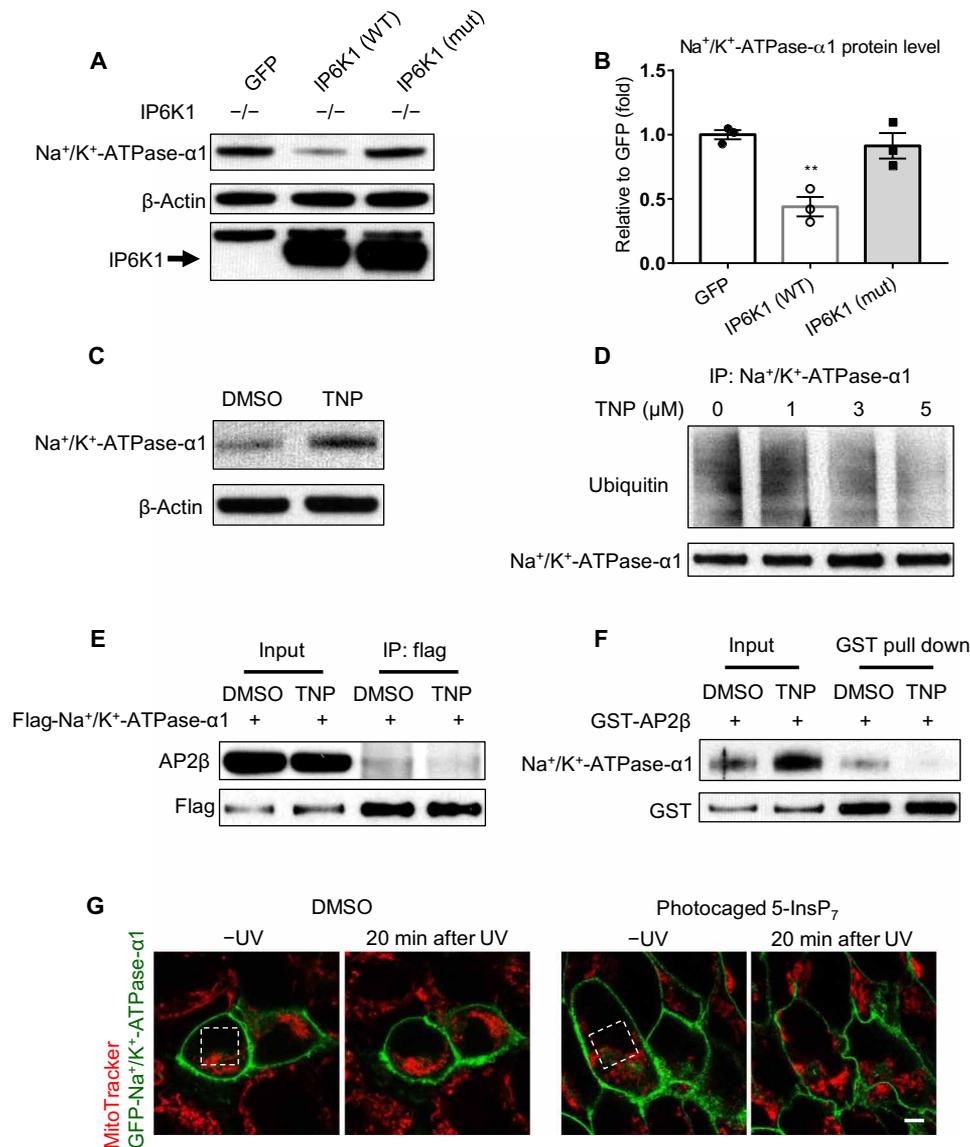
Fig. 3. Inositol pyrophosphates promote Na$^+$/K$^+$-ATPase-α1 endocytosis. (**A** and **B**) WT IP6K1, kinase-defective mutant (mut) IP6K1, or GFP (negative control) were overexpressed in *IP6K1* KO MEF cells to rescue the expression of IP6K1. Overexpression of WT, but not mut IP6K1, decreased Na$^+$/K$^+$-ATPase-α1 protein level ($n = 3$; normalized to β-actin). (**C**) Human embryonic kidney (HEK) 293 cells were treated with DMSO or N^2-(m-(trifluoromethyl)benzyl)N^6-(p-nitrobenzyl)purine (TNP; 3 μM) for 24 hours to inhibit 5-InsP$_7$ synthesis. TNP treatment increased Na$^+$/K$^+$-ATPase-α1 protein level. (**D**) HEK 293 cells were treated with increasing concentrations of TNP (0 μM, DMSO) for 24 hours. Na$^+$/K$^+$-ATPase-α1 was immunoprecipitated and blotted for ubiquitin. TNP treatment dose-dependently depleted Na$^+$/K$^+$-ATPase-α1 ubiquitination. (**E**) Flag-tagged Na$^+$/K$^+$-ATPase-α1 was overexpressed in HEK 293 cells. Cells were treated with DMSO or TNP (3 μM) for 24 hours. Flag-tagged Na$^+$/K$^+$-ATPase-α1 was immunoprecipitated by an anti-flag antibody and blotted for AP2β. The amount of coimmunoprecipitated AP2β was less in TNP-treated cells. (**F**) Glutathione S-transferase (GST)–fused AP2β (GST-AP2β) was overexpressed in HEK 293 cells. Cells were treated with DMSO or TNP (3 μM) for 24 hours. GST-AP2β was pulled down by Glutathione Sepharose and blotted for Na$^+$/K$^+$-ATPase-α1. Less Na$^+$/K$^+$-ATPase-α1 was pulled down in TNP-treated cells. (**G**) GFP-fused Na$^+$/K$^+$-ATPase-α1 was overexpressed in HEK 293 cells. Cells were incubated with DMSO or photocaged 5-InsP$_7$ for 4 hours and MitoTracker (red) for 30 min. Photochemical release of 5-InsP$_7$ by ultraviolet (UV) irradiation (dotted box) decreased GFP-Na$^+$/K$^+$-ATPase-α1 level in the plasma membrane. Nonilluminated neighboring cells were used as controls. Scale bar, 5 μm.

(Fig. 3D). These results indicate that IP6K1 promotes Na^+/K^+-ATPase-α1 degradation via its enzymatic product 5-InsP$_7$.

Next, we tested whether 5-InsP$_7$ is required for Na^+/K^+-ATPase-α1 endocytosis (Fig. 3, E to G). We treated human embryonic kidney (HEK) 293 cells with TNP to block 5-InsP$_7$ synthesis (Fig. 3, E and F). Immunoprecipitation of flag-tagged Na^+/K^+-ATPase-α1 pulled down less AP2 in TNP-treated cells (Fig. 3E). Similarly, glutathione S-transferase (GST) pull down of GST-fused AP2 coprecipitated less Na^+/K^+-ATPase-α1 in TNP-treated cells (Fig. 3F). Thus, inhibition of 5-InsP$_7$ synthesis by TNP treatment decreased interaction of Na^+/K^+-ATPase-α1 with AP2 (Fig. 3, E and F), which is required for Na^+/K^+-ATPase-α1 endocytosis.

To obtain direct evidence that 5-InsP$_7$ mediates Na^+/K^+-ATPase-α1 endocytosis, we overexpressed green fluorescent protein (GFP)–fused Na^+/K^+-ATPase-α1 in HEK 293 cells, and treated the cells with cell-permeant photocaged 5-InsP$_7$ (fig. S6C) (22) to observe its influence upon GFP-fused Na^+/K^+-ATPase-α1 in real time via confocal microscopy (Fig. 3G). GFP-fused Na^+/K^+-ATPase-α1 is mainly expressed in the cell membrane. Photochemical releasing of 5-InsP$_7$ depleted GFP-fused Na^+/K^+-ATPase-α1 levels, demonstrating that 5-InsP$_7$ directly drives Na^+/K^+-ATPase-α1 endocytosis (Fig. 3G).

5-InsP$_7$ mediates interaction between Na^+/K^+-ATPase-α1 and PI3K p85α

Endocytosis of Na^+/K^+-ATPase under pathological conditions involves phosphorylation of the α subunit (13). To test whether 5-InsP$_7$ drives physiological endocytosis of Na^+/K^+-ATPase-α1 by promoting its phosphorylation, we immunoprecipitated Na^+/K^+-ATPase-α1 and blotted for phospho-Na^+/K^+-ATPase-α1 at serine-16 and serine-23, which are critical for its endocytosis in response to dopamine (13). Phosphorylation of Na^+/K^+-ATPase-α1 at serine-16 and serine-23 was similar between WT and *IP6K1* KO preparations (fig. S6D). We also assessed whether 5-InsP$_7$ up-regulates the phosphorylation of AP2μ subunit at threonine-156, which can trigger AP2-mediated endocytosis (23). Phosphorylation of AP2μ did not differ between WT and *IP6K1* KO preparations (fig. S6E). Thus, 5-InsP$_7$ did not affect the phosphorylation of Na^+/K^+-ATPase-α1 nor the phosphorylation of AP2μ.

Next, we tested whether 5-InsP$_7$ mediates endocytosis of Na^+/K^+-ATPase-α1 via promoting its binding with PI3K p85α, which is a prerequisite for AP2 recruitment (14). Coimmunoprecipitation of Na^+/K^+-ATPase-α1 with PI3K p85α was markedly diminished in the *IP6K1* KO tissues (Fig. 4, A and B). Enzymatic activity of IP6K1 is required for promoting the interaction between Na^+/K^+-ATPase-α1 and PI3K p85α, because pharmacological inhibition of 5-InsP$_7$ synthesis by TNP treatment impaired the binding of Na^+/K^+-ATPase-α1 with PI3K p85α (Fig. 4, C and D). Thus, 5-InsP$_7$ mediates endocytosis of Na^+/K^+-ATPase-α1 via promoting its interaction with PI3K p85α.

We tested the possibility that IP6K1 acts as a scaffolding protein to coordinate a Na^+/K^+-ATPase-α1/PI3K p85α/AP2 protein complex by exploring the binding of IP6K1 with these proteins (Fig. 4E). We overexpressed myc-tagged IP6K1 in HEK 293 cells with myc-tagged GFP as a negative control (Fig. 4E). Myc-tagged IP6K1 coimmunoprecipitated PI3K p85α but not Na^+/K^+-ATPase-α1 nor AP2, suggesting that IP6K1 binds with PI3K p85α but not with Na^+/K^+-ATPase-α1 nor AP2 (Fig. 4E). These results indicate that while IP6K1 binds with PI3K p85α, it does not appear to act as a scaffolding protein to coordinate the interaction of PI3K p85α with Na^+/K^+-ATPase-α1. We confirmed the association of IP6K1 with PI3K

p85α by coimmunoprecipitation of IP6K1 and PI3K p85α in mice tissues (Fig. 4, F and G). To test whether binding of PI3K p85α to IP6K1 affects its enzymatic activity, we performed an in vitro assay and found that PI3K p85α did not alter IP6K1 enzymatic activity (fig. S7).

Inositol pyrophosphates enhance binding between Na^+/K^+-ATPase-α1 and PI3K p85α

We tested whether the interaction between PI3K p85α and Na^+/K^+-ATPase-α1 enhanced by IP6K1 is directly mediated by 5-InsP$_7$ in an in vitro binding assay (Fig. 5A). 5-InsP$_7$ increased the binding between PI3K p85α and Na^+/K^+-ATPase-α1 in a concentration-dependent manner, saturating at a physiological concentration of 5 μM (Fig. 5A). Inositol hexakisphosphate (InsP$_6$), which lacks the pyrophosphate at the 5-position of the inositol ring (fig. S8A), did not increase the binding of PI3K p85α with Na^+/K^+-ATPase-α1 (fig. S8B), demonstrating a requirement for the pyrophosphate moiety (fig. S8A).

To explore whether the position of pyrophosphate affects binding of PI3K p85α with Na^+/K^+-ATPase-α1, we tested 1-diphosphoinositol pentakisphosphate (1-InsP$_7$), 3-diphosphoinositol pentakisphosphate (3-InsP$_7$), and 5-InsP$_7$, which have the pyrophosphate at 1-, 3-, and 5-positions of the inositol ring, respectively (fig. S8A). 1-InsP$_7$ did not affect the binding of PI3K p85α with Na^+/K^+-ATPase-α1, but 3-InsP$_7$ and 5-InsP$_7$ increased the binding of PI3K p85α with Na^+/K^+-ATPase-α1 (fig. S8C), suggesting that the position of the pyrophosphate moiety on the inositol ring matters (fig. S8A).

Besides 5-InsP$_7$, IP6K1 has a minor product: diphosphoinositol tetrakisphosphate (5-PP-InsP$_4$) (24). 5-PP-InsP$_4$ has a pyrophosphate at the 5-position but lacks a phosphate at the 2-position (fig. S8A). 5-PP-InsP$_4$ did not enhance the binding between PI3K p85α and Na^+/K^+-ATPase-α1 (fig. S8D), demonstrating a requirement of phosphate at the 2-position of the inositol ring in addition to the pyrophosphate moiety (fig. S8A).

Because 5-InsP$_7$ functions by binding or pyrophosphorylating target proteins (2, 25), we tested whether protein pyrophosphorylation is involved in regulating the interaction of Na^+/K^+-ATPase-α1 with PI3K p85α by 5-InsP$_7$. We used 5-PCP-InsP$_5$ (5-PCP), a methylene-bisphosphonate nonhydrolyzable analog of 5-InsP$_7$ (26), and 5-PCF$_2$Am-InsP$_5$ (CF2), a fluorinated nonhydrolyzable analog of 5-InsP$_7$ (27). 5-PCP and CF2 closely mimic the physicochemical and biochemical properties of 5-InsP$_7$ (fig. S8A) but cannot transfer their β-phosphoryl groups onto protein substrates. Both 5-PCP and CF2 enhanced the binding of PI3K p85α with Na^+/K^+-ATPase-α1 (Fig. 5B), indicating that protein pyrophosphorylation is not involved. Similarly, 3-PCP-InsP$_5$ (3-PCP), a methylene-bisphosphonate non-hydrolyzable analog of 3-InsP$_7$ (fig. S8A) also increased binding of PI3K p85α with Na^+/K^+-ATPase-α1 (Fig. 5B), further confirming that protein pyrophosphorylation is not involved in mediating binding of PI3K p85α with Na^+/K^+-ATPase-α1 (fig. S8A).

5-InsP$_7$ disinhibits binding between PI3K p85α and Na^+/K^+-ATPase-α1

To obtain direct evidence of ligand binding by 5-InsP$_7$, we used 5-PCP-InsP$_5$ (5-PCP), a nonhydrolyzable analog of 5-InsP$_7$, as bait to pull down PI3K p85α and Na^+/K^+-ATPase-α1. 5-PCP was linked to resin by polyethylene glycol (PEG) at either the 2-position or 1/3-position of the inositol ring. 5-PCP resin pulled down PI3K p85α (Fig. 5C). The binding of 5-PCP resin with PI3K p85α seemed to be
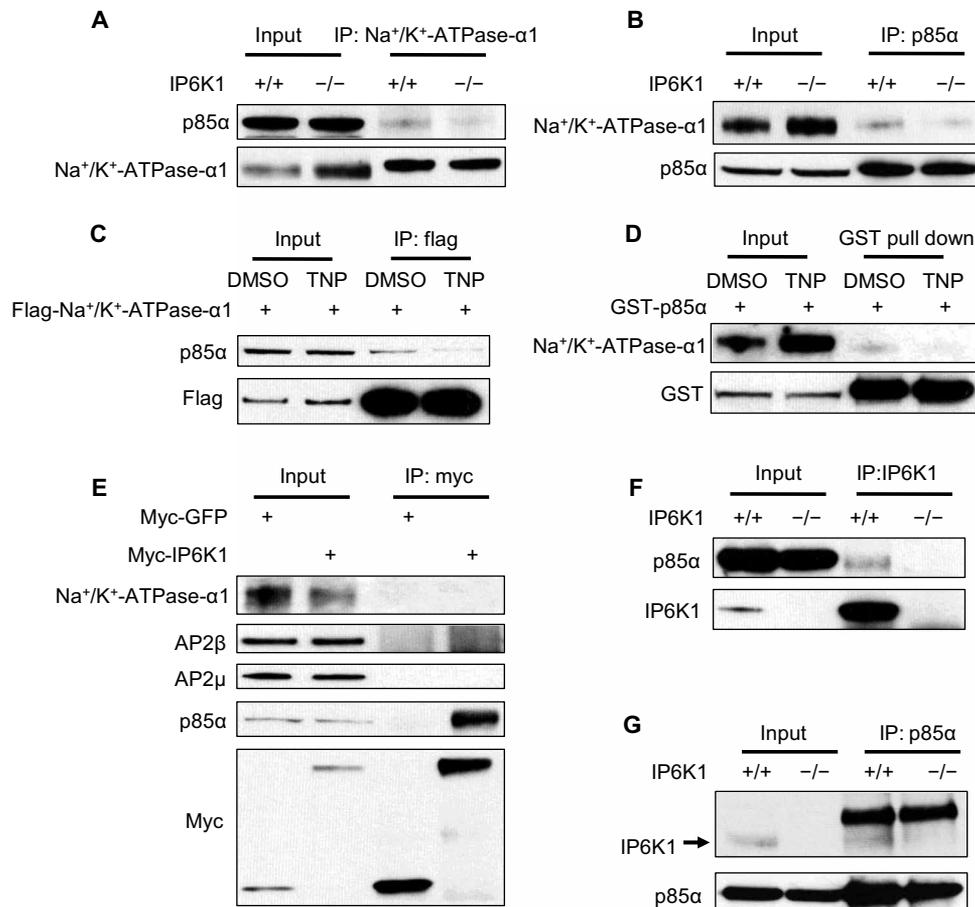
Fig. 4. IP6K1 mediates interaction between Na⁺/K⁺-ATPase-α1 and PI3K p85α. (**A** and **B**) Coimmunoprecipitation of Na⁺/K⁺-ATPase-α1 and PI3K p85α from WT and *IP6K1* KO mice kidneys. (A) Less PI3K p85α was co–pulled down by Na⁺/K⁺-ATPase-α1 in *IP6K1* KO preparations. (B) Less Na⁺/K⁺-ATPase-α1 was coprecipitated by PI3K p85α in *IP6K1* KO samples. (**C**) Flag-tagged Na⁺/K⁺-ATPase-α1 was overexpressed in HEK 293 cells. The cells were treated with TNP (3 μM) to block 5-InsP₇ synthesis for 24 hours. DMSO was used as the solvent control. Flag-tagged Na⁺/K⁺-ATPase-α1 was immunoprecipitated by an anti-flag antibody and blotted for PI3K p85α. The amount of coprecipitated PI3K p85α was less in TNP-treated cells. (**D**) GST-fused PI3K p85α (GST-p85α) was overexpressed in HEK 293 cells. The cells were treated with TNP (3 μM) for 24 hours. DMSO was used as the solvent control. GST-p85α was pulled down by Glutathione Sepharose and blotted for Na⁺/K⁺-ATPase-α1. Less Na⁺/K⁺-ATPase-α1 was co–pulled down in TNP-treated cells. (**E**) Myc-tagged IP6K1 was overexpressed in HEK 293 cells. Myc-tagged GFP was overexpressed in separate HEK 293 cells as negative control. Myc-tagged IP6K1 and myc-tagged GFP were pulled down by an anti-myc antibody. Myc-tagged IP6K1 co–pulled down PI3K p85α but not Na⁺/K⁺-ATPase-α1, AP2β, nor AP2μ. (**F** and **G**) Coimmunoprecipitation of IP6K1 and PI3K p85α in WT and *IP6K1* KO kidneys. (F) PI3K p85α was coimmunoprecipitated by IP6K1 in WT preparations only. (G) IP6K1 was co–pulled down by PI3K p85α in WT samples.

affected by the position of the inositol ring where the PEG linker is attached because only 5-PCP resin linked to the symmetrical 5-PCP-InsP₅ via a PEG linker attached to the 1/3-phosphates, thus effectively creating a chirally discriminated ligand (fig. S9A) (*28*), but not the 2-phosphate of the inositol ring (*29*) pulled down PI3K p85α (Fig. 5C). 5-PCP resin failed to pull down Na⁺/K⁺-ATPase-α1 (fig. S9B). This result suggests that 5-InsP₇ participates in a protein-ligand interaction with PI3K p85α that presumably induces a conformational change to promote an interaction with Na⁺/K⁺-ATPase-α1 rather than acting as a "molecular glue" for PI3K p85α and Na⁺/K⁺-ATPase-α1. Further insight into the structural basis of protein-ligand interactions requires solving a structure, but we hypothesize a model of the structure-activity relationship based on data from analog and resin experiments (fig. S10).

To identify the specific region of PI3K p85α that binds 5-InsP₇, we expressed different domains of PI3K p85α in HEK 293 cells. 5-PCP resin pulled down the RhoGAP domain but not the SH3 (Src

homology 3 domain) or SH2 motifs (Fig. 5D). To confirm that the RhoGAP domain of PI3K p85α is responsible for binding 5-InsP₇, we deleted the RhoGAP domain from PI3K p85α (ΔRhoGAP) and found that 5-PCP resin did not bind ΔRhoGAP mut PI3K p85α (Fig. 5E).

Does the RhoGAP domain affect the binding of PI3K p85α with Na⁺/K⁺-ATPase-α1? To answer this, we performed an in vitro binding assay to compare full-length (FL) PI3K p85α with ΔRhoGAP mut PI3K p85α for their ability to bind Na⁺/K⁺-ATPase-α1 (Fig. 5F). ΔRhoGAP mut PI3K p85α pulled down more Na⁺/K⁺-ATPase-α1 than FL PI3K p85α did and to a level similar to FL PI3K p85α in the presence of CF2 (Fig. 5F). This demonstrates that deleting the RhoGAP domain potentiates the ability of PI3K p85α to bind Na⁺/K⁺-ATPase-α1. Our results show that the RhoGAP domain of PI3K p85α autoinhibits its interaction with Na⁺/K⁺-ATPase-α1, and binding of 5-InsP₇ to the RhoGAP domain relieves this autoinhibition.

To further confirm that 5-InsP₇ targets the RhoGAP domain of PI3K p85α to promote Na⁺/K⁺-ATPase-α1 degradation, we tested
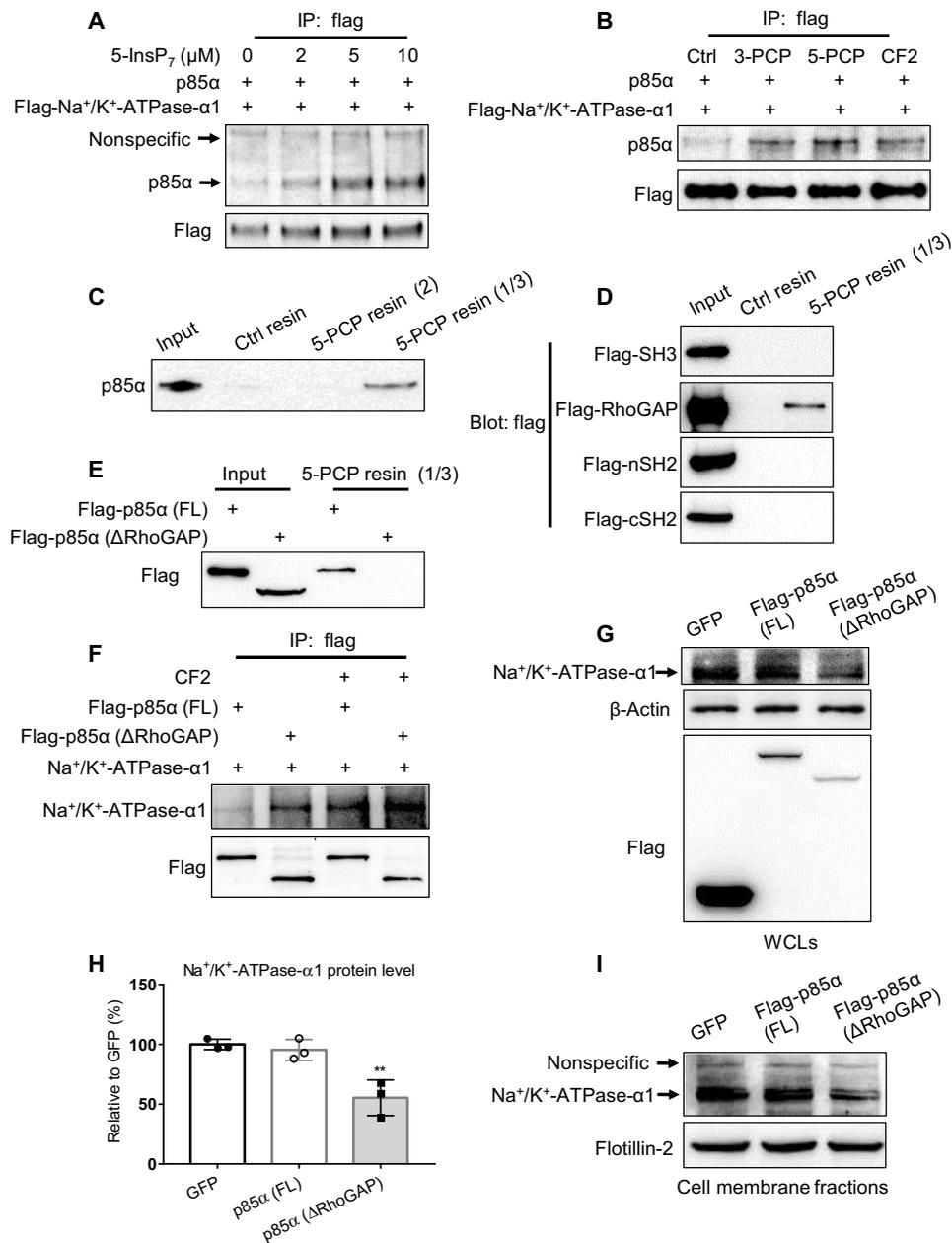
Fig. 5. 5-InsP$_7$ disinhibits binding between PI3K p85α and Na$^+$/K$^+$-ATPase-α1. (**A** and **B**) Flag-tagged Na$^+$/K$^+$-ATPase-α1 immunoprecipitated on protein A/G beads was incubated with PI3K p85α in the presence of (A) increasing concentrations of 5-InsP$_7$ and (B) 5 μM 3-PCP, 5-PCP, or CF2. Binding between Na$^+$/K$^+$-ATPase-α1 and PI3K p85 was enhanced by 5-InsP$_7$, 3-PCP, 5-PCP, and CF2. (**C**) PI3K p85α was incubated with control resin, 2-position–linked 5-PCP resin [5-PCP resin (2)], or 1/3-position–linked 5-PCP resin [5-PCP resin (1/3)]. PI3K p85α was pulled down by 5-PCP resin (1/3) but not by 5-PCP resin (2). (**D**) Flag-tagged domains of PI3K p85α (SH3, RhoGAP, nSH2, and cSH2) were overexpressed in HEK 293 cells. Whole-cell lysates were incubated with 5-PCP resin (1/3), which only pulled down flag-tagged RhoGAP. (**E**) Flag-tagged full-length (FL) PI3K p85α and flag-tagged RhoGAP domain–deleted (ΔRhoGAP) PI3K p85α were overexpressed in HEK 293 cells. Whole-cell lysates were incubated with 5-PCP resin (1/3), which pulled down flag-tagged FL PI3K p85α but not flag-tagged ΔRhoGAP PI3K p85α. (**F**) Flag-tagged FL PI3K p85α and flag-tagged ΔRhoGAP PI3K p85α immunoprecipitated on protein A/G beads were incubated with Na$^+$/K$^+$-ATPase-α1. Flag-tagged ΔRhoGAP PI3K p85α pulled down more Na$^+$/K$^+$-ATPase-α1 than flag-tagged FL PI3K p85α did (without CF2) and to a level similar to flag-tagged FL PI3K p85α in the presence of CF2. (**G** to **I**) Overexpression of flag-tagged ΔRhoGAP PI3K p85α in HEK 293 cells reduced Na$^+$/K$^+$-ATPase-α1 protein level in whole-cell lysates (WCLs) [(G) and (H), $n = 3$; normalized to β-actin] and membrane fractions (I).

whether overexpression of the ΔRhoGAP mut PI3K p85α decreases Na$^+$/K$^+$-ATPase-α1 protein level. Overexpressing ΔRhoGAP PI3K p85α substantially reduced protein levels of Na$^+$/K$^+$-ATPase-α1 in both whole-cell preparations (Fig. 5, G and H) and cell membrane fractions (Fig. 5I). The working model is shown in Fig. 6.

DISCUSSION

This study reveals a previously unidentified and fundamental role of 5-InsP$_7$ as a potent, endogenous small-molecule destabilizer of Na$^+$/K$^+$-ATPase. We began by comparing the cell membrane proteins between WT and *IP6K1* KO MEF cells. We found that deletion

of IP6K1 elicits a twofold increase in Na$^+$/K$^+$-ATPase-α1, the principal Na$^+$/K$^+$-ATPase catalytic subunit expressed in multiple tissues and cell types. The increased protein level of Na$^+$/K$^+$-ATPase-α1 in *IP6K1* KO mice is associated with greater renal Na$^+$ reabsorption during HS diets. We found that ubiquitination of Na$^+$/K$^+$-ATPase-α1 was decreased in *IP6K1* KO cells. IP6K1 deletion reduced endocytosis of Na$^+$/K$^+$-ATPase-α1 from the cell membrane. Recruitment of AP2 to Na$^+$/K$^+$-ATPase-α1, which drives its internalization into endocytic vesicles, was disrupted in *IP6K1* KO cells. Endocytosis of Na$^+$/K$^+$-ATPase-α1 requires its binding with PI3K p85α (*14*), which was disrupted in *IP6K1* KO cells. Mechanistically, we found that IP6K1 associates with PI3K p85α and generates 5-InsP$_7$ that binds the PI3K p85α RhoGAP domain in a stereoselective manner. Although IP6K1 protein itself is unlikely to be required per se, the lack of regulation by IP6K2 and IP6K3 indicates that specifically IP6K1-generated 5-InsP$_7$ regulates Na$^+$/K$^+$-ATPase-α1. The isoform-specific regulation and IP6K1/PI3K p85α binding support a local 5-InsP$_7$ pool model (*9*). We show that 5-InsP$_7$ potentiates binding between PI3K p85α and Na$^+$/K$^+$-ATPase-α1 by relieving the autoinhibitory function of the RhoGAP domain in a pyrophosphorylation-independent manner, which triggers endocytosis and downstream degradation of Na$^+$/K$^+$-ATPase-α1 (Fig. 6). Binding of 5-InsP$_7$ to the RhoGAP domain presumably causes a conformational rearrangement to relieve the autoinhibition. Because the SH3 domain of PI3K p85α binds to a proline-rich region of Na$^+$/K$^+$-ATPase-α1 (*14*), the structural basis of autoinhibition by the RhoGAP domain may involve disruption of this interaction. Structural biology studies are warranted to fully elucidate these interactions.

IP6K1 has been proposed as a metabolic sensor in pancreatic β cells to link ATP/ADP (adenosine 5′-diphosphate) ratio and insulin secretion by regulating 5-InsP$_7$ levels (*30*). We propose that IP6K1 may also function as an ATP sensor to maintain homeostatic levels of Na$^+$/K$^+$-ATPase-α1. Physiologically, IP6K1 robustly generates 5-InsP$_7$ to mediate Na$^+$/K$^+$-ATPase-α1 endocytosis and degradation in a steady-state manner. When ATP levels are decreased, synthesis of 5-InsP$_7$ by IP6K1 is suppressed to maintain electrochemical gradients by stabilizing Na$^+$/K$^+$-ATPase-α1. This hypothesis is supported by the fact that the protein level of Na$^+$/K$^+$-ATPase-α1 subunit transiently increases after acute ischemia (*31*), and temporary decreases of cellular ATP level does not inhibit Na$^+$ reabsorption by the proximal tubule cells (*32*). 5-InsP$_7$ negatively regulates intracellular ATP levels by altering the glycolytic/mitochondrial metabolic ratio (*33*). Thus, depleting 5-InsP$_7$ by TNP treatment will increase intracellular ATP level, fueling the activity of Na$^+$/K$^+$-ATPase. It should be noted that other Na$^+$/K$^+$-ATPase isoforms exist beyond α1 and β1 that are expressed in a tissue-specific manner (*18*). While we did not address them, IP6K1 may also regulate other Na$^+$/K$^+$-ATPase isoforms in certain tissues.

5-InsP$_7$ is further phosphorylated by diphosphoinositol pentakisphosphate kinases to form 1,5-bis-diphosphoinositol 2,3,4,6-tetrakisphosphate (1,5-InsP$_8$), which has diphosphates at both 1- and 5-positions of the inositol ring (*5*). We have demonstrated that 5-InsP$_7$ but not InsP$_6$ nor 1-InsP$_7$ promoted the interaction of PI3K p85α with Na$^+$/K$^+$-ATPase-α1, indicating that a diphosphate at the 5-position is required. However, we did not exclude the possibility that 1,5-InsP$_8$ could also play a role in mediating the binding of PI3K p85α with Na$^+$/K$^+$-ATPase-α1. Both 5-InsP$_7$ and 1,5-InsP$_8$ are closely linked to cellular energy homeostasis, however, under different mechanisms. The intracellular ATP level increases fourfold in 5-InsP$_7$–depleted cells (*33*), whereas it elevates 35% in 1,5-InsP$_8$–
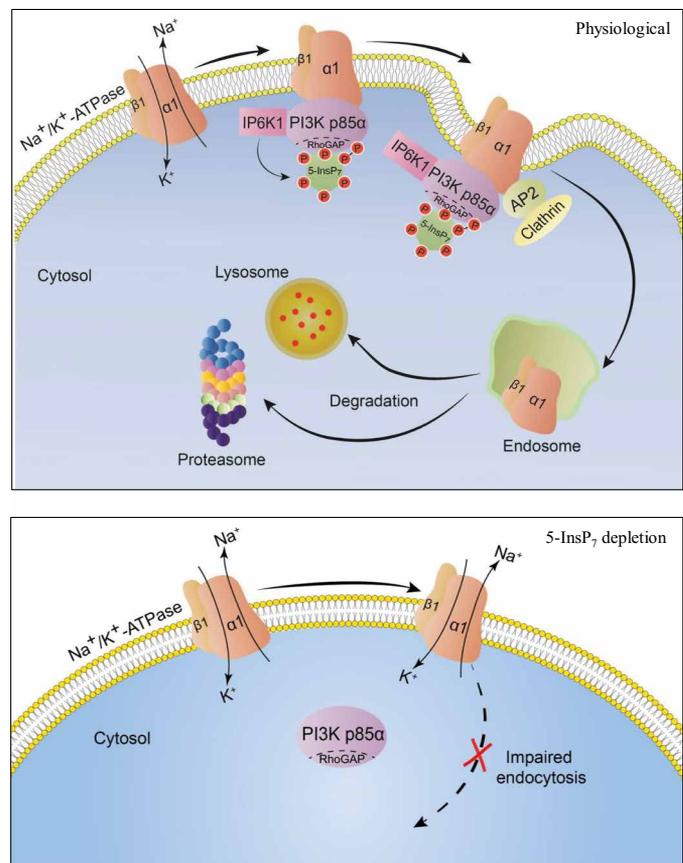
Fig. 6. Model for 5-InsP$_7$ regulation of Na$^+$/K$^+$-ATPase-α1 endocytosis and downstream degradation. (**Top**) IP6K1 physiologically associates with PI3K p85α and generates a local pool of 5-InsP$_7$, which binds the RhoGAP domain of PI3K p85α. Binding of 5-InsP$_7$ with PI3K p85α disinhibits the interaction between PI3K p85α and Na$^+$/K$^+$-ATPase-α1. This recruits AP2, which mediates clathrin-mediated endocytosis and leads to downstream degradation of Na$^+$/K$^+$-ATPase-α1. (**Bottom**) Depleting 5-InsP$_7$ disrupts the binding between PI3K p85α and Na$^+$/K$^+$-ATPase-α1, which impairs recruitment of endocytic machinery and downstream degradation.

depleted cells (*34*). ATP promotes 5-InsP$_7$ but not 1,5- InsP$_8$ synthesis (*34, 35*). If 1,5-InsP$_8$ can regulate Na$^+$/K$^+$-ATPase-α1, then it would be most detectable across cells with variable basal 5-InsP$_7$ levels, 1,5-InsP$_8$ phosphatase activities, or extracellular conditions that modulate flux through the inositol phosphate synthesis pathway. Nonetheless, the physiological concentration of 1,5-InsP$_8$ is much lower than that of 5-InsP$_7$ (*3*).

Regulation of Na$^+$/K$^+$-ATPase is complex, which is necessary to maintain appropriate tissue functions and homeostasis under physiological and pathophysiological conditions (*11*). Disturbance of the Na$^+$/K$^+$-ATPase-α1 has been reported in many diseases, including cancer, diabetes, and heart failure (*11*). Despite decades of research, the identification of endogenous digitalis-like factors has been elusive (*17*). We found that 5-InsP$_7$ is an endogenous negative regulator of Na$^+$/K$^+$-ATPase-α1. The Na$^+$/K$^+$-ATPase modulators demonstrate therapeutic efficacy in conditions such as cardiovascular diseases (*36*) and cancers (*37*). We anticipate that our finding will have broad therapeutic applications.

MATERIALS AND METHODS

Cell culture and transfection

HEK 293 cells, HEK 293T cells, WT MEF cells, and *IP6K1* KO MEF cells were cultured in Dulbecco's Modified Eagle Medium (DMEM) medium (Thermo Fisher Scientific) supplemented with 10% (v/v) fetal bovine serum (FBS; Gemini BenchMark), penicillin (100 U/ml), and streptomycin (100 µg/ml) (Thermo Fisher Scientific). hRPTCs were cultured in DMEM-F12 media (Invitrogen) supplemented with 2% FBS, plasmocin (5 µg/ml; InvivoGen), epidermal growth factor (10 ng/ml; MilliporeSigma), dexamethasone (36 ng/ml; MilliporeSigma), triiodothyronine (2 ng/ml; MilliporeSigma), 1× insulin/transferrin/selenium (Invitrogen), penicillin (100 U/ml) and streptomycin (100 µg/ml), and G418 sulfate (0.2 mg/ml; EMD Chemicals). All cells were maintained at 37°C with 5% CO_2. Cells were plated 1 day before the experiments. Before treating cells, the existing cell culture medium was exchanged with fresh medium. Transfections were conducted with Lipofectamine 3000 (Thermo Fisher Scientific). *IP6K1* knockdown hRPTCs were generated by shRNA transfection. Cycloheximide and TNP were purchased from MilliporeSigma.

Western blotting and immunoprecipitation

Tissues and cells were homogenized by pestle at 4°C in a lysis buffer containing 50 mM tris-HCl (pH 7.4), 100 mM NaCl, 0.5% Igepal CA630, 5 mM $MgCl_2$, and protease/phosphatase inhibitors (MilliporeSigma). Lysates were pulse sonicated and centrifuged at 14,000*g* for 10 min at 4°C. Protein concentrations were normalized using the Pierce BCA Protein Assay Kit (Thermo Fisher Scientific). SDS loading buffer (1×) (Invitrogen) containing 5% β-mercaptoethanol was added, and the samples were boiled for 5 min.

For immunoprecipitation, tissues and cells were homogenized by pestle at 4°C in the aforementioned lysis buffer. Lysates were passed through 30-gauge needles 20 times and centrifuged at 14,000*g* for 10 min at 4°C. The supernatants were collected and precleaned with protein A/G beads (Santa Cruz Biotechnology) for 90 min at 4°C. Lysates were centrifuged briefly, and the supernatants were collected while the protein A/G beads were discarded. Primary antibody was added to cell lysates and incubated at 4°C overnight. Protein A/G beads were then added to the cell lysates and incubated for 2 hours at 4°C. The beads were washed with cold lysis buffer three times. SDS loading buffer (1.5×) containing 5% β-mercaptoethanol was added, and the samples were boiled for 5 min.

Samples were run on 4 to 12% polyacrylamide bis-tris gradient gels (Invitrogen) in MES running buffer (Invitrogen) and transferred to nitrocellulose membranes (Bio-Rad). Membranes were blocked with 5% milk in TBST (tris-buffered saline with 1% Triton X-100), or 5% bovine serum albumin (BSA) (Thermo Fisher Scientific) in TBST for phospho-antibodies, for 30 min at room temperature, washed with TBST, and incubated with primary antibodies in 5% BSA in TBST overnight at 4°C. The following day, membranes were washed with TBST, incubated with secondary antibodies for 1 hour at room temperature, and washed again with TBST. Chemiluminescent substrate (Thermo Fisher Scientific) was used to visualize protein bands by film.

Antibodies against IP6K1, myc-tag (clone 9E10), flag-tag (clone M2), and GST were purchased from MilliporeSigma. Antibodies against pan-cadherin, β-actin, PI3K p85α, Na^+/K^+-ATPase β1, and flotillin-2 were purchased from Cell Signaling Technology. Antibodies against Na^+/K^+-ATPase-α1 and ubiquitin were purchased from Santa Cruz Biotechnology. Antibody against AP2β was purchased

from Bethyl Laboratories. Antibodies against AP2µ and phospho-AP2µ (T156) were purchased from Abcam. Alexa Fluor 568 goat anti-rabbit and Alexa Fluor 488 goat anti-mouse immunoglobulin G (IgG) were purchased from Thermo Fisher Scientific.

Subcellular fractionation

Cell membrane fractions were isolated by ultracentrifuge. Tissues and cells were homogenized by pestle at 4°C in buffer containing 250 mM sucrose, 20 mM Hepes (pH 7.4), 10 mM KCl, 1.5 mM $MgCl_2$, 1 mM EDTA, 1 mM EGTA, 1 mM dithiothreitol (DTT), and protease/phosphatase inhibitors. Lysates were passed through a 30-gauge needle 20 times, incubated on ice for 20 min, and centrifuged at 14,000*g* for 20 min at 4°C. The supernatant was collected and centrifuged at 200,000*g* for 2 hours at 4°C. The resulting supernatant was the cytosolic fraction. The pellet left was washed with fractionation buffer, resuspended by pipetting, and recentrifuged at 200,000*g* for 2 hours at 4°C. The resulting pellet was the membrane fraction, which contains plasma membrane, microsomes, and small vesicles.

Endocytic vesicles were isolated, as reported (*38*). Tissues were lysed in a glass homogenizer on ice with 20 strokes in a lysis buffer containing 100 mM MES (pH 6.5), 0.2 mM EGTA, 0.5 mM $MgCl_2$, and protease/phosphatase inhibitors. The lysates were centrifuged at 4100*g* for 32 min at 4°C. The supernatant was collected, supplemented with ribonuclease A (50 µg/ml), and incubated for 1 hour at 4°C. The lysates were centrifuged at 210,000*g* for 40 min at 4°C. The resulting pellet was resuspended with the same lysis buffer and mixed with equal amounts of cold buffer containing 100 mM MES (pH 6.5), 0.2 mM EGTA, 0.5 mM $MgCl_2$, 12.5% (w/v) Ficoll PM400 (GE Healthcare), 12.5% (w/v) sucrose, and protease/phosphatase inhibitors. The suspensions were centrifuged at 22,000*g* for 30 min at 4°C. The supernatants were collected, mixed with four volumes of lysis buffer, and centrifuged at 121,000*g* for 45 min. The resulting pellet, which contains the endocytic vesicles–enriched fraction, was collected.

Animal experiments

WT, *IP6K1* KO, and *IP6K2* KO mice were littermates from heterozygous breeding. Animal breeding and procedures were conducted in accordance with the National Institutes of Health *Guide for Care and Use of Laboratory Animals* and approved by the Animal Care and Use Committee of the Johns Hopkins University School of Medicine. All in vivo experiments were performed with adult (6- to 8-months) male age-matched mice.

NS diet (Teklad 2018SX) was the standard chow diet at the Johns Hopkins University School of Medicine mouse facility ("X" denotes extruded instead of compressed pellets). HS diet (Teklad 2018S 4% NaCl; TD.130254) was given to mice for 9 weeks.

Mice were habituated in metabolic cages (Techniplast) for 2 days, returned back to normal cages for 2 days, and placed back into the metabolic cages for 3 days. Urine was collected during the final 24 hours. Mineral oil, removed afterward via centrifugation, was added into the collection tube to prevent error due to evaporation. After recording volume, urine samples were analyzed for electrolyte concentrations by the Johns Hopkins Hospital Pathology services.

Blood was collected into lithium heparin tubes (Becton Dickinson) from WT and *IP6K1* KO mice via cardiac puncture. Blood was added to i-STAT CHEM8+ cartridges, and values were obtained from an i-STAT machine (Abaxis).

Histology

Mice were euthanized by CO_2 and transcardially perfused with phosphate-buffered saline (PBS) followed by 4% (w/v) paraformaldehyde. Kidneys were excised and fixed in 4% (w/v) paraformaldehyde for at least 48 hours. H&E, PAS, and Masson staining were conducted by the Johns Hopkins Hospital Pathology services.

Immunostaining

Animals were perfused and fixed with 4% (w/v) paraformaldehyde. Mouse renal sections or cultured cells were washed with PBS followed by fixation with 4% (w/v) paraformaldehyde. The samples were blocked with 10% (v/v) goat serum (MilliporeSigma) for 10 min at room temperature and then incubated with primary antibodies at 4°C overnight. The samples were washed multiple times with PBS for 3 hours at room temperature and then incubated with fluorescent-dye conjugated secondary antibodies for 1 hour at room temperature. Nuclei were stained with Hoechst 33342 (Thermo Fisher Scientific) for 10 min. Proximal tubules were stained by incubating with fluorescein-labeled *Lotus tetragonolobus* Lectin (LTL) (Vector Laboratories) for 2 hours. Slices were mounted with ProLong Gold Antifade Mountant (Thermo Fisher Scientific). Pictures were taken under a confocal microscope (Zeiss LSM 700).

Measurement of FITC-inulin in plasma

Fluorescein isothiocyanate (FITC)–inulin 5% (w/v) (MilliporeSigma) was dissolved in normal saline and dialyzed. The solution was sterilized by filtration through a 0.22-μm syringe filter. Mice were anesthetized briefly by isoflurane. FITC-inulin solution (2 μl/g of body weight) was injected into the retro-orbital plexus using a 30-gauge needle. Mice tails were cut, and blood was collected from the tails at 3, 5, 7, 10, 15, 35, 56, and 75 min after injection. The plasma was diluted 1:20 with 0.5 M Hepes (pH 7.4). Normal mouse plasma was collected from mice of the same background strain and diluted 1:20 with 0.5 M Hepes (pH 7.4). A standard plasma FITC-inulin solution was made by serial dilution of FITC-inulin with diluted mouse plasma. Fluorescence was determined using an EnSpire Multimode Plate Reader (PerkinElmer) with 485-nm excitation and read at 538-nm emission (*39*).

RNA isolation and real-time PCR

Total RNA was isolated from mice tissues and cells using the RNeasy Mini Kit (Qiagen) and reverse transcribed to complementary DNA using SuperScript III (Invitrogen) according to the manufacturer's recommended protocol. Real-time quantitative PCR was performed with the TaqMan Gene Expression Master Mix and the Step One Plus instrument (Life Technologies). β-Actin was used as a loading control.

Plasmid cloning

Myc-tagged GFP, myc-tagged WT IP6K1, myc-tagged kinase-defective mut IP6K1 (K226A), flag-tagged PI3K p85α, flag-tagged ΔRhoGAP PI3K p85α, flag-tagged SH3 domain of PI3K p85α, flag-tagged RhoGAP domain of PI3K p85α, flag-tagged nSH2 domain of PI3K p85α, flag-tagged cSH2 domain of PI3K p85α, GST-fused PI3K p85α, flag-tagged Na^+/K^+-ATPase-α1, GST-fused Na^+/K^+-ATPase-α1, GST-fused AP2β, and GST-fused GFP were cloned into the pCDH-EF1-MCS-T2A-copGFP vector (System Biosciences). Na^+/K^+-ATPase-α1 was cloned into pLVX-AcGFP1-N1 vector (Takara Bio) to make GFP-fused Na^+/K^+-ATPase-α1. The PCR products were generated by using Phusion Polymerase (Thermo Fisher Scientific) and inserted into the vectors using the In-Fusion HD Enzyme (Takara Bio). IP6K1 shRNA and scramble control shRNA plasmids were purchased from MilliporeSigma. All newly constructed plasmids were sequence verified.

Lentivirus generation

HEK 293T cells were plated 1 day before the experiments and allowed to grow to 70% confluence. Lentiviral vectors harboring the gene of interest together with pMD2.G and psPAX2 were transfected into HEK 293T cells using Lipofectamine 3000. Cell culture medium was replaced with fresh medium 4 hours after transfection. The virus-containing medium was collected 48 hours later and filtered through a 0.48-μm filter and then mixed with 1/2 volume of concentration medium containing 25.5% PEG 6000 (MilliporeSigma), 0.9 M NaCl, 2.5 mM sodium phosphate buffer, and 0.4 mM KH_2PO_4. The samples were stored at 4°C overnight then centrifuged at 17,000*g* for 1 hour at 4°C. The resulting pellet containing lentivirus was resuspended with DMEM medium and stored at −80°C (*40*).

Biotin labeling

Biotinylation was performed using the Pierce Cell Surface Protein Isolation Kit (Thermo Fisher Scientific). MEF cells plated on 35-mm glass-bottom plates (MatTEK) were washed twice with ice-cold PBS^{2+}/BSA [PBS supplemented with 1.5 mM $MgCl_2$, 0.2 mM $CaCl_2$, 0.18% (w/v) glucose, and 0.2% (w/v) BSA]. EZ-Link Sulfo-NHS-SS-Biotin was diluted in PBS^{2+}/BSA (0.25 mg/ml) and added onto MEF cells for 30 min on a rotator at 4°C. Quenching solution was added [biotin solution (50 μl/ml)] to the cells and incubated for 15 min. The cells culture medium was changed with PBS^{2+}/BSA and incubated at 37°C for 3 hours. Cells were washed with PBS followed by fixation with 4% (w/v) paraformaldehyde (Electron Microscopy Sciences). The samples were blocked with 10% (v/v) goat serum (MilliporeSigma) for 10 min and then with anti–Na^+/K^+-ATPase-α1 primary antibody at 4°C overnight. The samples were washed multiple times with PBS for 3 hours at room temperature and then incubated with the Alexa Fluor 568–conjugated F(ab′)₂-Goat anti-Mouse IgG (Life Technologies) for 1 hour at room temperature. The samples were washed with PBS for 3 hours at room temperature, incubated with DyLight 488 Streptavidin (BioLegend) for 30 min at room temperature, and washed with PBS for 1 hour at room temperature. Nuclei were stained with Hoechst 33342 (Thermo Fisher Scientific) for 10 min.

Photocaged 5-InsP₇ induced Na^+/K^+-ATPase-α1 endocytosis

The photocaged 5-InsP₇ was synthesized, as reported (*22*). Acetoxy-benzyl (AB) groups at the inositol phosphate esters reversibly mask the phosphate and their negative charge, thus enabling diffusion into cells. Inside the cells, the AB groups are quickly removed by esterases, thereby releasing photocaged 5-InsP₇. The caging group [7-(diethylamino)coumarin-4-yl]methyl is positioned on the β-phosphate of the phosphoric anhydride of 5-InsP₇ and can be removed on demand with a laser pulse releasing the active second messenger 5-InsP₇ on a second time scale. HEK 293 cells were grown to 70% confluence on 35-mm glass-bottom plates (MatTEK). GFP-fused Na^+/K^+-ATPase-α1 was overexpressed in HEK 293 cells by lentiviral transduction. Cells were then incubated for 48 hours. The cell culture media were then replaced with fresh media and incubated with 5 μM photocaged 5-InsP₇ or dimethyl sulfoxide (DMSO) for 4 hours and MitoTracker (100 nM) for 30 min. After incubation, the medium was removed, and cells were washed with PBS and replaced

with phenol red–free DMEM (Thermo Fisher Scientific) for imaging. Imaging was performed on a confocal microscope (Zeiss LSM 700), and cells were kept at ambient temperature. An image of GFP-fused Na^+/K^+-ATPase-α1 was captured before illumination. Cells were irradiated at wavelength of 405 nm on predefined square regions of 5 to 10 μm length to release 5-$InsP_7$ photochemically. The GFP-fused Na^+/K^+-ATPase-α1 in the cell membrane was captured after 2 s of irradiation within the regions of interest. This cycle was repeated every minute for 20 min. Nonilluminated neighboring cells were used as controls.

Small-molecule synthesis
5-PP-$InsP_4$, 5-PCF_2Am-$InsP_5$, and 5-PCP-$InsP_5$ were synthesized as previously described (26, 27, 41). 3-PCP-$InsP_5$ was synthesized as previously described for 1,5-$[PCP]_2$-$InsP_4$ but starting from 1D-6-O-benzyl-1,2:4,5-di-O-isopropylidene *myo*-inositol (42). The inositol pyrophosphates 1-$InsP_7$, 3-$InsP_7$, and 5-$InsP_7$ were synthesized using similar methods to those previously described (43, 44). All synthetic compounds were purified by ion-exchange chromatography, fully characterized by ^1H, ^{31}P, and ^{13}C nuclear magnetic resonance (NMR) spectroscopy and, where feasible, quantified by total phosphate analysis. Commercially available $InsP_6$ (MilliporeSigma) was used.

Inositol pyrophosphate affinity reagent synthesis
2-Position 5-PCP-$InsP_5$ resin was synthesized as previously described (29). 1/3-Position 5-PCP-$InsP_5$ resin was synthesized as previously described (28).

In vitro binding assay
To assess the binding of Na^+/K^+-ATPase-α1 with PI3K p85α, flag-tagged Na^+/K^+-ATPase-α1 and GST-fused PI3K p85α were overexpressed in HEK 293 cells. Cell lysates were precleaned with protein A/G beads (Santa Cruz Biotechnology), and anti-flag-tag antibody was added to cell lysates expressing flag-tagged Na^+/K^+-ATPase-α1 overnight. Flag-tagged Na^+/K^+-ATPase-α1 was pulled down by protein A/G beads and washed for three times. Separately, Glutathione Sepharose (GE Life Sciences) was used to pull down GST-fused PI3K p85α, and PreScission Protease (GE Life Sciences) was applied to cleave GST and release PI3K p85α into buffer. Buffer with purified PI3K p85α was added to protein A/G agarose–bound flag-tagged Na^+/K^+-ATPase-α1 in the presence of different inositol phosphates overnight at 4°C. Beads were then collected and washed three times. The samples were loaded with 1.5× SDS loading buffer containing 5% β-mercaptoethanol and boiled for 5 min.

To assess the binding of PI3K p85α to 5-PCP-$InsP_5$, the control and 5-PCP-$InsP_5$ resin were equilibrated with cell lysis buffer. The amount of immobilized species on the resin was made equal by normalizing the yield, which was obtained via NMR as previously described (29). PI3K p85α, prepared from GST-fused PI3K p85α via Glutathione Sepharose and PreScission Protease, was added onto the 5-PCP-$InsP_5$ resin and incubated overnight at 4°C. The resins were collected and washed three times. The samples were mixed with 1.5× SDS loading buffer containing 5% β-mercaptoethanol and boiled for 5 min.

The flag-tagged domains of PI3K p85α were overexpressed in HEK 293 cells. 5-PCP-$InsP_5$ resin was equilibrated with cell lysis buffer and incubated cell lysates overnight at 4°C. The resins were washed with lysis buffer for three times. The samples were mixed with 1.5× SDS loading buffer containing 5% β-mercaptoethanol and boiled for 5 min. Free Na^+/K^+-ATPase-α1 was prepared from HEK 293 cells by PreScission Protease cleavage of GST.

In vitro enzymatic assays
Na^+/K^+-ATPase activity was measured using the Na^+/K^+-ATPase Microplate Assay Kit (Cohesion Biosciences). WT and *IP6K1* KO kidneys were lysed and treated with or without ouabain (MilliporeSigma). Following incubation at 37°C for 80 min, the ATPase reaction was stopped. Dye was added to measure inorganic phosphate, and absorbance readings were obtained on a microplate reader (Molecular Devices). Na^+/K^+-ATPase activity was calculated by subtracting the reading from the ouabain-treated sample from that of the control sample. Results are presented as fold change of WT.

IP6K1 activity was measured using the ADP-Glo Max Assay Kit (Promega). GST-fused PI3K p85α, GST-fused IP6K1, and GST-fused GFP were overexpressed in HEK 293 cells and harvested by Glutathione Sepharose. PreScission Protease was used to cleave the GST and release PI3K p85α, IP6K1, and GFP into a buffer containing 50 mM tris (pH 7.4), 10 mM $MgCl_2$, and 2.5 mM DTT. IP6K1 activity assay was conducted in a reaction containing protein (~20 mg/ml) (1:1 ratio of IP6K1:GFP or 1:1 ratio of IP6K1:PI3K p85α), 50 μM $InsP_6$, and 100 μM ATP for 2 hours at 37°C. The reaction was quenched with ADP-Glo Reagent for 40 min, and the ADP-Glo Max Detection Reagent was added and incubated for 60 min. Using an opaque white 96-well plate (Costar), bioluminescent signal in relative light units was obtained on a microplate reader with an integration time of 1 s per well (45).

Statistical analysis
All data are presented as means ± SEM. Unpaired two-tailed Student's *t* test was used to test for significance when comparing the data. Differences were considered significant at *$P < 0.05$, **$P < 0.01$, and ***$P < 0.001$ (ns, not significant).

SUPPLEMENTARY MATERIALS
Supplementary material for this article is available at http://advances.sciencemag.org/cgi/content/full/6/44/eabb8542/DC1

View/request a protocol for this paper from *Bio-protocol*.

REFERENCES AND NOTES
1. M. J. Berridge, P. Lipp, M. D. Bootman, The versatility and universality of calcium signalling. *Nat. Rev. Mol. Cell Biol.* **1**, 11–21 (2000).
2. M. S. Wilson, T. M. Livermore, A. Saiardi, Inositol pyrophosphates: Between signalling and metabolism. *Biochem. J.* **452**, 369–379 (2013).
3. S. B. Shears, Diphosphoinositol polyphosphates: Metabolic messengers? *Mol. Pharmacol.* **76**, 236–252 (2009).
4. A. Chakraborty, S. Kim, S. H. Snyder, Inositol pyrophosphates as mammalian cell signals. *Sci. Signal.* **4**, re1 (2011).
5. S. B. Shears, Intimate connections: Inositol pyrophosphates at the interface of metabolic regulation and cell signaling. *J. Cell. Physiol.* **233**, 1897–1912 (2018).
6. A. Chakraborty, The inositol pyrophosphate pathway in health and diseases. *Biol. Rev. Camb. Philos. Soc.* **93**, 1203–1227 (2018).
7. F. Rao, J. Xu, C. Fu, J. Y. Cha, M. M. Gadalla, R. Xu, J. C. Barrow, S. H. Snyder, Inositol pyrophosphates promote tumor growth and metastasis by antagonizing liver kinase B1. *Proc. Natl. Acad. Sci. U.S.A.* **112**, 1773–1778 (2015).
8. T. Rojas, W. Cheng, Z. Gao, X. Liu, Y. Wang, A. P. Malla, A. C. Chin, L. H. Romer, S. H. Snyder, C. Fu, Inositol hexakisphosphate kinase 3 promotes focal adhesion turnover via interactions with dynein intermediate chain 2. *Proc. Natl. Acad. Sci. U.S.A.* **116**, 3278–3287 (2019).
9. S. B. Shears, Inositol pyrophosphates: Why so many phosphates? *Adv. Biol. Regul.* **57**, 203–216 (2015).
10. C. Gatto, S. M. McLoud, J. H. Kaplan, Heterologous expression of Na^+-K^+-ATPase in insect cells: Intracellular distribution of pump subunits. *Am. J. Physiol. Cell Physiol.* **281**, C982–C992 (2001).

11. M. V. Clausen, F. Hilbers, H. Poulsen, The structure and function of the Na$^+$,K$^+$-ATPase isoforms in health and disease. *Front. Physiol.* **8**, 371 (2017).

12. E. Lecuona, H. Sun, C. Vohwinkel, A. Ciechanover, J. I. Sznajder, Ubiquitination participates in the lysosomal degradation of Na,K-ATPase in steady-state conditions. *Am. J. Respir. Cell Mol. Biol.* **41**, 671–679 (2009).

13. A. V. Chibalin, C. H. Pedemonte, A. I. Katz, E. Féraille, P. O. Berggren, A. M. Bertorello, Phosphorylation of the catalytic α-subunit constitutes a triggering signal for Na$^+$,K$^+$-ATPase endocytosis. *J. Biol. Chem.* **273**, 8814–8819 (1998).

14. G. A. Yudowski, R. Efendiev, C. H. Pedemonte, A. I. Katz, P. O. Berggren, A. M. Bertorello, Phosphoinositide-3 kinase binds to a proline-rich motif in the Na$^+$,K$^+$-ATPase α subunit and regulates its trafficking. *Proc. Natl. Acad. Sci. U.S.A.* **97**, 6556–6561 (2000).

15. G. Ogimoto, G. A. Yudowski, C. J. Barker, M. Köhler, A. I. Katz, E. Féraille, C. H. Pedemonte, P.-O. Berggren, A. M. Bertorello, G protein-coupled receptors regulate Na$^+$,K$^+$-ATPase activity and endocytosis by modulating the recruitment of adaptor protein 2 and clathrin. *Proc. Natl. Acad. Sci. U.S.A.* **97**, 3242–3247 (2000).

16. A. P. Comellas, L. A. Dada, E. Lecuona, L. M. Pesce, N. S. Chandel, N. Quesada, G. R. S. Budinger, G. J. Strous, A. Ciechanover, J. I. Sznajder, Hypoxia-mediated degradation of Na,K-ATPase via mitochondrial reactive oxygen species and the ubiquitin-conjugating system. *Circ. Res.* **98**, 1314–1322 (2006).

17. V. M. Buckalew, Endogenous digitalis-like factors: An overview of the history. *Front. Endocrinol.* **6**, 49 (2015).

18. G. Blanco, R. W. Mercer, Isozymes of the Na-K-ATPase: Heterogeneity in structure, diversity in function. *Am. J. Physiol.* **275**, F633–F650 (1998).

19. M. Liang, J. Tian, L. Liu, S. Pierre, J. Liu, J. Shapiro, Z.-J. Xie, Identification of a pool of non-pumping Na/K-ATPase. *J. Biol. Chem.* **282**, 10585–10593 (2007).

20. A. Chakraborty, M. A. Koldobskiy, N. T. Bello, M. Maxwell, J. J. Potter, K. R. Juluri, D. Maag, S. Kim, A. S. Huang, M. J. Dailey, M. Saleh, A. M. Snowman, T. H. Moran, E. Mezey, S. H. Snyder, Inositol pyrophosphates inhibit Akt signaling, thereby regulating insulin sensitivity and weight gain. *Cell* **143**, 897–910 (2010).

21. U. Padmanabhan, D. E. Dollins, P. C. Fridy, J. D. York, C. P. Downes, Characterization of a selective inhibitor of inositol hexakisphosphate kinases: Use in defining biological roles and metabolic relationships of inositol pyrophosphates. *J. Biol. Chem.* **284**, 10571–10582 (2009).

22. S. Hauke, A. K. Dutta, V. B. Eisenbeis, D. Bezold, T. Bittner, C. Wittwer, D. Thakor, I. Pavlovic, C. Schultz, H. J. Jessen, Photolysis of cell-permeant caged inositol pyrophosphates controls oscillations of cytosolic calcium in a β-cell line. *Chem. Sci.* **10**, 2687–2692 (2019).

23. O. Olusanya, P. D. Andrews, J. R. Swedlow, E. Smythe, Phosphorylation of threonine 156 of the μ2 subunit of the AP2 complex is essential for endocytosis in vitro and in vivo. *Curr. Biol.* **11**, 896–900 (2001).

24. A. Saiardi, J. J. Caffrey, S. H. Snyder, S. B. Shears, The inositol hexakisphosphate kinase family. Catalytic flexibility and function in yeast vacuole biogenesis. *J. Biol. Chem.* **275**, 24686–24692 (2000).

25. A. Saiardi, R. Bhandari, A. C. Resnick, A. M. Snowman, S. H. Snyder, Phosphorylation of proteins by inositol pyrophosphates. *Science* **306**, 2101–2105 (2004).

26. M. Wu, B. E. Dul, A. J. Trevisan, D. Fiedler, Synthesis and characterization of non-hydrolysable diphosphoinositol polyphosphate second messengers. *Chem. Sci.* **4**, 405–410 (2013).

27. A. M. Riley, H. Wang, S. B. Shears, B. V. L. Potter, Synthesis of an α-phosphono-α,α-difluoroacetamide analogue of the diphosphoinositol pentakisphosphate 5-InsP$_7$. *MedChemComm* **10**, 1165–1172 (2019).

28. D. Furkert, S. Hostachy, M. Nadler-Holly, D. Fiedler, Triplexed affinity reagents to sample the mammalian inositol pyrophosphate interactome. *Cell Chem. Biol.* **27**, 1097–1108.e4 (2020).

29. M. Wu, L. S. Chong, D. H. Perlman, A. C. Resnick, D. Fiedler, Inositol polyphosphates intersect with signaling and metabolic networks via two distinct mechanisms. *Proc. Natl. Acad. Sci. U.S.A.* **113**, E6757–E6765 (2016).

30. S. S. Rajasekaran, J. Kim, G.-C. Gaboardi, J. Gromada, S. B. Shears, K. T. D. Santos, E. L. Nolasco, S. de Souza Ferreira, C. Illies, M. Köhler, C. Gu, S. H. Ryu, J. O. Martins, E. Darè, C. J. Barker, P.-O. Berggren, Inositol hexakisphosphate kinase 1 is a metabolic sensor in pancreatic β-cells. *Cell. Signal.* **46**, 120–128 (2018).

31. M. J. Kim, J. Hur, I.-H. Ham, H. J. Yang, Y. Kim, S. Park, Y.-W. Cho, Expression and activity of the Na-K ATPase in ischemic injury of primary cultured astrocytes. *Korean J. Physiol. Pharmacol.* **17**, 275–281 (2013).

32. C. Coor, R. F. Salmon, R. Quigley, D. Marver, M. Baum, Role of adenosine triphosphate (ATP) and NaK ATPase in the inhibition of proximal tubule transport with intracellular cystine loading. *J. Clin. Invest.* **87**, 955–961 (1991).

33. Z. Szijgyarto, A. Garedew, C. Azevedo, A. Saiardi, Influence of inositol pyrophosphates on cellular energy dynamics. *Science* **334**, 802–805 (2011).

34. C. Gu, H.-N. Nguyen, D. Ganini, Z. Chen, H. J. Jessen, Z. Gu, H. Wang, S. B. Shears, KO of 5-InsP$_7$ kinase activity transforms the HCT116 colon cancer cell line into a hypermetabolic, growth-inhibited phenotype. *Proc. Natl. Acad. Sci. U.S.A.* **114**, 11968–11973 (2017).

35. K. Choi, E. Mollapour, J. H. Choi, S. B. Shears, Cellular energetic status supervises the synthesis of bis-diphosphoinositol tetrakisphosphate independently of AMP-activated protein kinase. *Mol. Pharmacol.* **74**, 527–536 (2008).

36. Y. Yan, J. I. Shapiro, The physiological and clinical importance of sodium potassium ATPase in cardiovascular diseases. *Curr. Opin. Pharmacol.* **27**, 43–49 (2016).

37. H.-Y. Wang, G. A. O'Doherty, Modulators of Na/K-ATPase: A patent review. *Expert Opin. Ther. Pat.* **22**, 587–605 (2012).

38. G. H. Borner, A. B. Fielding, Isolating HeLa cell fractions enriched for clathrin-coated vesicles. *Cold Spring Harb. Protoc.* **2014**, 1184–1187 (2014).

39. T. Rieg, A High-throughput method for measurement of glomerular filtration rate in conscious mice. *J. Vis. Exp.* **2013**, e50330 (2013).

40. R. H. Kutner, X.-Y. Zhang, J. Reiser, Production, concentration and titration of pseudotyped HIV-1-based lentiviral vectors. *Nat. Protoc.* **4**, 495–505 (2009).

41. H. Wang, H. Y. Godage, A. M. Riley, J. D. Weaver, S. B. Shears, B. V. L. Potter, Synthetic inositol phosphate analogs reveal that PPIP5K2 has a surface-mounted substrate capture site that is a target for drug discovery. *Chem. Biol.* **21**, 689–699 (2014).

42. A. M. Riley, H. Wang, S. B. Shears, B. V. L. Potter, Synthetic tools for studying the chemical biology of InsP$_8$. *Chem. Commun.* **51**, 12605–12608 (2015).

43. S. Capolicchio, D. T. Thakor, A. Linden, H. J. Jessen, Synthesis of unsymmetric diphospho-inositol polyphosphates. *Angew. Chem. Int. Ed. Engl.* **52**, 6912–6916 (2013).

44. I. Pavlovic, D. T. Thakor, L. Bigler, M. S. C. Wilson, D. Laha, G. Schaaf, A. Saiardi, H. J. Jessen, Prometabolites of 5-Diphospho-*myo*-inositol Pentakisphosphate. *Angew. Chem. Int. Ed. Engl.* **54**, 9622–9626 (2015).

45. M. Wormald, G. Liao, M. Kimos, J. Barrow, H. Wei, Development of a homogenous high-throughput assay for inositol hexakisphosphate kinase 1 activity. *PLOS ONE* **12**, e0188852 (2017).

ScienceAdvances

The inositol pyrophosphate 5-InsP$_7$ drives sodium-potassium pump degradation by relieving an autoinhibitory domain of PI3K p85 α

Alfred C. Chin, Zhe Gao, Andrew M. Riley, David Furkert, Christopher Wittwer, Amit Dutta, Tomas Rojas, Evan R. Semenza, Robin A. Felder, Jennifer L. Pluznick, Henning J. Jessen, Dorothea Fiedler, Barry V. L. Potter, Solomon H. Snyder and Chenglai Fu

ARTICLE TOOLS	http://advances.sciencemag.org/content/6/44/eabb8542
SUPPLEMENTARY MATERIALS	http://advances.sciencemag.org/content/suppl/2020/10/26/6.44.eabb8542.DC1
REFERENCES	This article cites 45 articles, 17 of which you can access for free http://advances.sciencemag.org/content/6/44/eabb8542#BIBL
PERMISSIONS	http://www.sciencemag.org/help/reprints-and-permissions

Use of this article is subject to the Terms of Service